ice | proceedings

Humidity buffering using stabilised rammed earth materials

David Allinson MSc, PhD
Senior Research Associate, School of Civil and Building Engineering,
Loughborough University, Leicestershire, UK

Matthew Hall BSc, PhD, CSci, CEng, MIMMM, MInstP
Associate Professor in Materials Engineering, Nottingham Centre for
Geomechanics, University of Nottingham, Nottingham, UK

The humidity buffering potential of stabilised rammed earth materials is investigated based on the moisture buffer value concept. The moisture buffer value is (a) measured experimentally, (b) calculated from an analytical solution of the mass transfer and (c) simulated using a numerical solution of the combined heat and mass transfer. The numerical solution to the equations is described, as well as the modelling tool termed 'CHAMP' (coupled heat and mass transport in porous media). The results show that stabilised rammed earth can be a 'good' moisture buffering material under the Nordtest classification scheme. They also show that the moisture buffer value of stabilised rammed earth materials could be optimised or maximised by controlling the grading and mineralogy of the sub-soil and the manufacturing techniques. Sensitivity analysis of the moisture buffer value to the moisture transfer resistance at the surface is explored through numerical simulation and the need to control the experimental measurement carefully is explored.

Notation

A_s	area of surface (m^2)
b_m	moisture effusivity ($kg/(m^2\,Pa\,s^{1/2})$)
c_{pl}	constant pressure specific heat capacity (water) ($J/kg\,K$)
c_{pm}	constant pressure specific heat capacity (dry material) ($J/kg\,K$)
g	total rate of mass transfer ($kg/s\,m^2$)
g_l	rate of liquid water transfer ($kg/s\,m^2$)
g_v	rate of water vapour transfer ($kg/s\,m^2$)
h_e	specific latent enthalpy of evaporation (or condensation) (J/kg)
$MBV_{practical}$	measured moisture buffer value ($g/m^2\%RH$)
MBV_{ideal}	analytical moisture buffer value ($g/m^2\%RH$)
$MBV_{simulation}$	simulated moisture buffer value ($g/m^2\%RH$)
m	mass (g)
m_f	moisture factor for thermal conductivity
P_0	standard atmospheric pressure (barometric) (Pa)
P_a	total air pressure (Pa)
p_{sat}	saturation vapour pressure (Pa)
p_v	partial pressure of water vapour (Pa)
q	total heat flux (W/m^2)
q_{lat}	latent heat flux (W/m^2)
q_{sens}	sensible heat flux (W/m^2)
R	thermal resistance ($m^2\,K/W$)
RH	relative humidity ($\%$)
R_v	resistance to water vapour transfer ($m^2\,s\,Pa/kg_v$)
R_{vap}	individual gas constant of water vapour ($J/kg\,K$)
T	thermodynamic temperature (K)
t	time (s)
t_p	time period (s)
w	specific moisture content (kg/m^3)
w_m	moisture content (kg/kg)
x	one-dimensional distance (m)
δ_a	water vapour permeability of still air ($kg/m\,s\,Pa$)
δ_p	water vapour permeability ($kg/m\,s\,Pa$)
λ^*	moisture-dependent thermal conductivity ($W/m\,K$)
μ	water vapour diffusion resistance factor
ξ	moisture capacity (kg/kg)
ρ_d	dry density (kg/m^3)
φ	relative humidity (decimal)

1. Introduction

Humidity buffering occurs when porous building materials modify the relative humidity of indoor air, through absorption, storage and desorption of water vapour. This reduces the magnitude of relative humidity fluctuations in the same way that thermal mass reduces temperature swings. Excess water vapour inside buildings can originate from the occupants themselves (e.g. respiration and perspiration) and from their activities (e.g. cooking and washing). Buildings are traditionally designed so that this moisture can be removed by natural or mechanical

Construction Materials
Volume 165 Issue CM6

**Humidity buffering using
stabilised rammed earth
materials**
Allinson and Hall

ventilation. Significantly, the desire to improve the energy efficiency of buildings may lead to a reduction in the ventilation rate in some cases and many building materials are finished with vapour-resistant coatings (e.g. paint and vinyl wallpaper), which can lead to problems with moisture accumulation (Oreszczyn *et al.*, 2006). Equally, the heating and/or air conditioning of buildings can produce problematic low-humidity indoor environments. Carefully selected, humidity buffering building materials could be used to even out these daily or seasonal variations.

Research into humidity buffering materials has been motivated by a number of factors: the thermal comfort of building occupants is closely related to the humidity of the indoor air (Fang *et al.*, 1998a, 1998b; Kurnitski *et al.*, 2007; Simonson *et al.*, 2002); certain environments require tight humidity control to prevent damage to their contents (e.g. historic buildings, museums and art galleries) (Padfield, 1998); excessive humidity can promote dust mite populations and the growth of unsightly mould, both of which are known to be allergens with potentially serious health effects (Howieson, 2003; Oreszczyn *et al.* 2006); condensation and damp can significantly reduce the life of building materials; and finally, passive control of humidity by the fabric of the building may reduce or even remove the need for mechanical air conditioning, reducing the amount of energy required (Osanyintola and Simonson, 2006) as well as the running cost of the building. The moisture buffer value (MBV) is a single parameter that can be used to describe and compare the humidity buffering potential of building materials (Rode, 2005).

Stabilised rammed earth (SRE) is a traditional building technique in which moistened sub-soil material is dynamically compacted into formwork to create monolithic wall structures. Stabilisation, to improve durability and strength, is achieved through modification of the soil properties. Typically, in modern practice, this entails the addition of Portland cement in quantities up to 10% by mass. The technique is well established and used around the world and it may be considered a sustainable material with low embodied energy, especially when the sub-soil is sourced locally (Mendonca, 2007). SRE is also known (anecdotally) for its passive air-conditioning ability, that is the occupants of SRE buildings enjoy improved thermal comfort through the passive moderation of indoor temperature and humidity fluctuations (Minke, 2000; Mortenson, 2000; Taylor and Luther 2004). These abilities can perhaps be attributed to the combined effects of the thermal mass (air temperature buffering) of the material and its humidity buffering potential.

Quantifying the speculated humidity buffering potential of SRE is the subject of this paper. The MBV of three contrasting SRE materials, with a range of hygrothermal functional properties, was determined by experiment, analytical calculation and numerical simulation. The results were compared with other building materials. The numerical model, developed by the authors for this study, was used to explore the sensitivity of the results to variations in surface moisture transfer resistance. In this way, the paper demonstrates different methodologies that can be used to assess the moisture buffering ability of any porous building materials. It also quantifies the largely qualitative assessment that SRE is a good humidity buffering material.

2. Stabilised rammed earth materials and sample preparation

Stabilised rammed earth materials demonstrate a wide range of material properties that depend on the type of soil used (mineralogy and particle size distribution), the type and amount of binder, the energy used in compaction and the moisture content at compaction. Three different SRE materials, named after the mass proportions of a sand, a gravel and a silty clay that were combined to make the samples, were used for this investigation: 613, 433 and 703. Therefore, 613 SRE was manufactured from a mix of 60% sand, 10% gravel and 30% silty clay, by dry mass. The sand, gravel and silty clay were sourced from quarries located in the same geological area. Further characteristics and physical properties of these SRE mix designs can be found elsewhere (Hall and Djerbib, 2004).

The SRE samples used for the MBV tests were 'disc type' with dia. 105 mm and approximately 40 mm high. All were compacted using the same compaction energy and at the optimal moisture content, which was determined as 8%wt by BS 1377-4:1990 Proctor light (BSI, 1990). They were cured for a minimum of 28 days at 20°C and 75% relative humidity. In this way reproducible samples of different SRE materials could be manufactured. This provided a range of physical structures (density, porosity and void size distribution) which resulted in a range of hygrothermal functional properties: moisture-dependent thermal conductivity; moisture-dependent volumetric heat capacity; moisture storage function (sorption/desorption isotherms); and liquid and vapour permeability coefficients. The measurement of these properties has been described elsewhere (Hall and Allinson, 2009) and the results are summarised in Table 1.

3. Experimental measurement of MBV

The MBV of the SRE materials was measured after the Nordtest technique (Rode, 2005). This involved measuring the change in mass that resulted from repeatedly exposing one surface of the samples to 8 h in a high-humidity environment (nominally 75% RH) followed by 16 h in a low humidity (nominally 33% RH) under constant temperature (nominally 23°C±2) conditions. This was achieved using two small climate boxes that contained saturated solutions of sodium chloride (NaCl) and magnesium chloride ($MgCl_2$) to provide the specified humidity steps of 75% and 33%, respectively. They were located in a larger (walk-in)

Construction Materials
Volume 165 Issue CM6

**Humidity buffering using
stabilised rammed earth
materials**
Allinson and Hall

Material	Density, ρ_d: kg/m³	Heat capacity: c_{pm}: J/kg K	Thermal conductivity, λ: W/m K	Moisture factor, m_f	Moisture capacity, ξ: kg/kg	Water vapour permeability, δ_p: kg/m s Pa
613 SRE	2020	868·3	0·83	0·00245	0·01186	$1·27 \times 10^{-11}$
433 SRE	2120	868·3	1·01	0·0034	0·01292	$5·75 \times 10^{-12}$
703 SRE	1980	868·3	0·87	0·00322	0·00890	$1·88 \times 10^{-11}$
Gypsum board	1000[a]	840[b]	0·16[b]	0	0·03100	$2·50 \times 10^{-11}$ [a]
Brick	1600[a]	800[b]	0·62[b]	0	0·00240	$3·00 \times 10^{-11}$ [a]
Spruce boards	430[a]	2300[b]	0·12[b]	0	0·19005	$1·50 \times 10^{-12}$ [a]

[a]Values from Nordtest (Rode, 2005).
[b]Values from CIBSE Guide A (CIBSE, 2006).

Table 1. Functional properties of the materials

insulated chamber that was maintained at 23℃ by a thermostatic controller, an electrical natural convection heater and a fan. The SRE test sample was placed on an electronic balance (accuracy $\pm$ 0·01 g) that was incorporated under a special lid so that it could be placed in each of the climate boxes in turn. The sides and base of the specimens were sealed with a combination of a two-part epoxy resin adhesive and aluminium tape. A low-voltage fan was incorporated into the lid to ensure a steady air flow over the specimen surface and a 'Tinytag' data logger (accuracy: $\pm 0·5$℃ $\pm 2\%$ RH) recorded temperature and relative humidity at 10 min intervals. The output from the balance was recorded every minute by way of an RS232 cable attached to a personal computer (PC). A schematic diagram of the test set-up is shown in Figure 1. The specimens were conditioned at 23℃ and 50% RH before the test. The test duration depended upon the required equilibration period and was typically 5 days.

The MBV (MBV$_{practical}$) was calculated from the average of the mass gained by the sample during absorption (in 75% RH climate) and the mass lost during the subsequent desorption phase (33% RH climate), as shown in Figure 2. This change in mass was divided by the exposed area of the sample and the difference in relative humidity between the two environments, as shown in Equation 1. The quoted values of MBV$_{practical}$ were the average of three consecutive results

1. $$\text{MBV}_{practical} = \frac{\Delta m}{A_s \Delta \text{RH}}$$

A limitation of the technique was that the climate did not respond quickly to the sudden variations in relative humidity that occurred when the specimen was transferred from one environment to the other. Figure 3 shows the recorded
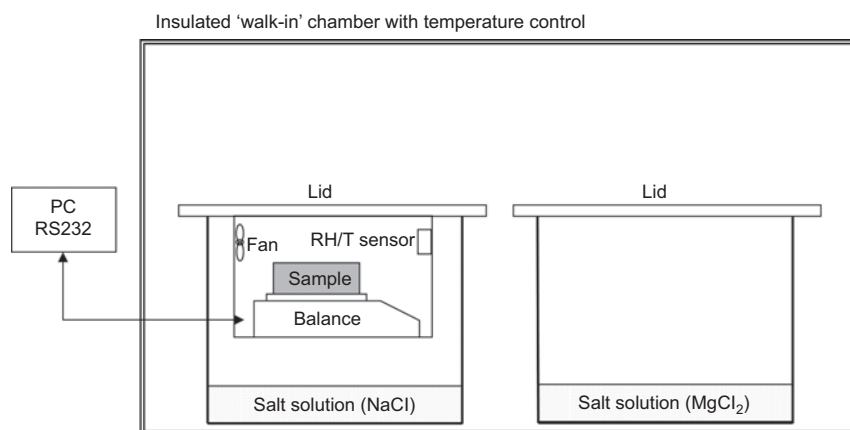

Insulated 'walk-in' chamber with temperature control

Figure 1. Schematic diagram of the MBV measurement set-up

Construction Materials
Volume 165 Issue CM6

**Humidity buffering using
stabilised rammed earth
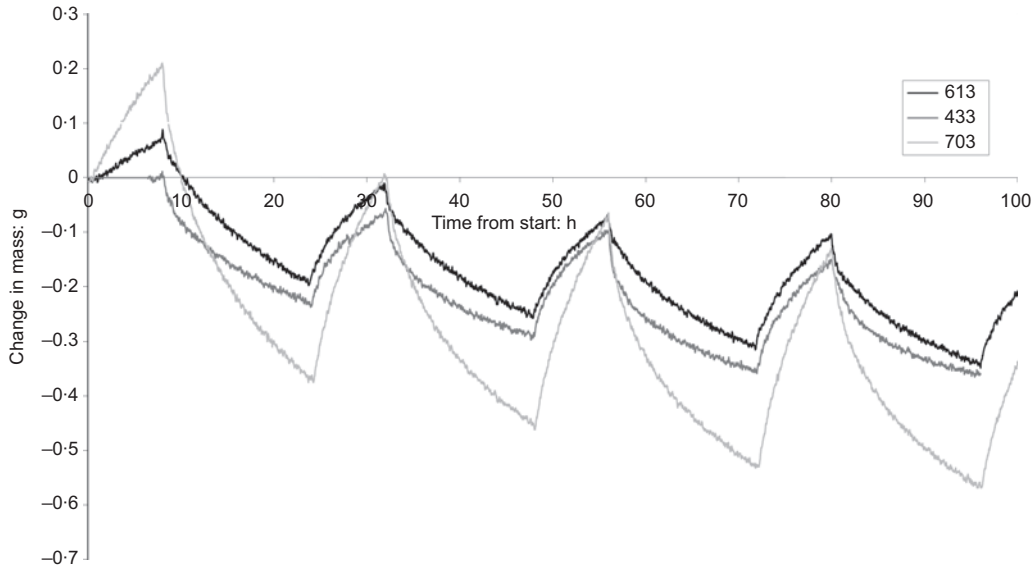materials**
Allinson and Hall

Figure 2. Recorded mass–time profiles for the MBV measurement
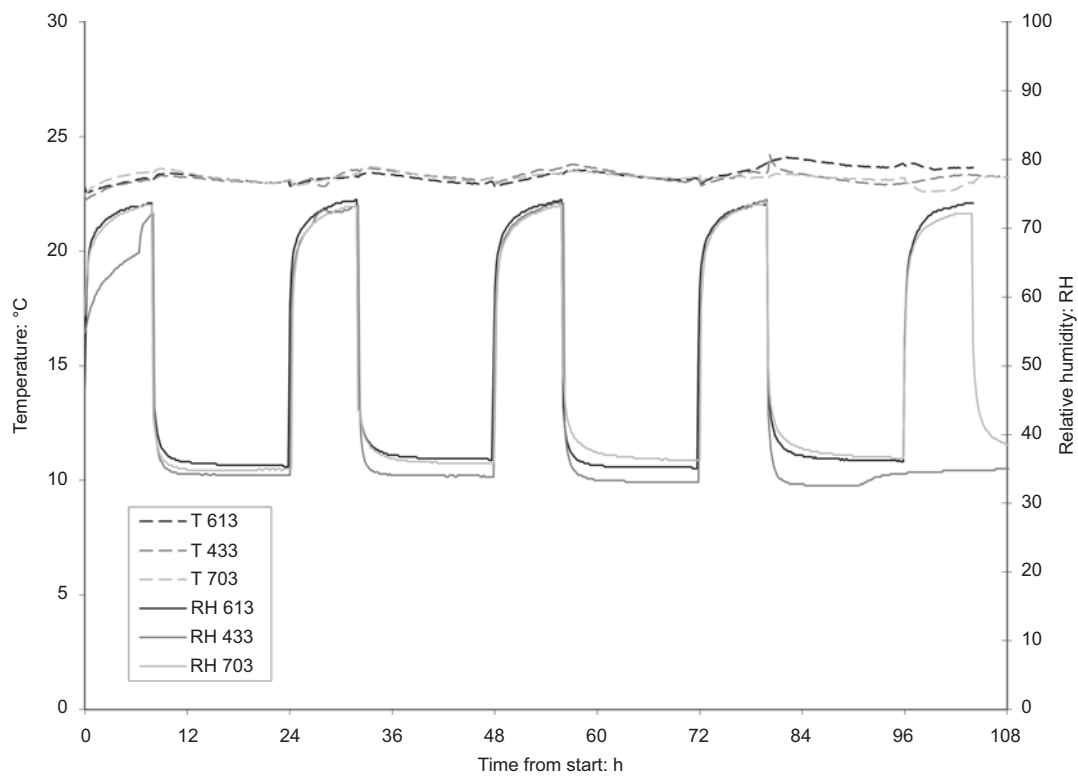
Figure 3. Recorded relative humidity and temperature profiles for
the MBV measurement

Construction Materials
Volume 165 Issue CM6

Humidity buffering using
stabilised rammed earth
materials
Allinson and Hall

temperature and relative humidity: the air temperature remained stable and the relative humidity, although slow to respond to each step change, achieved acceptable values in relation to the target set point. The maximum and minimum achieved values of relative humidity were used in the calculation of MBV$_{practical}$, although it should be recognised that specimens were never exposed to these relative humidity values for the full duration of each time step. In this way the calculated MBV$_{practical}$ values are likely to be conservative.

The repeatability of the MBV measurement has been explored in previous research by inter-laboratory round robin testing which showed that results varied by up to about 20% (Rode, 2005). This may be due (at least in part) to the sensitivity of the result to the near-surface air film resistance and the difficulty in controlling the air flow over the specimen; an issue which is explored later in this paper.

4. Analytical calculation of MBV

An analytical method for calculating the MBV from standard material properties was defined by the Nordtest project (Rode, 2005) as shown in Equation 2

2. $\text{MBV}_{ideal} = 0 \cdot 00568 p_s b_m \sqrt{t_p}$

The value of the material effusivity is calculated by Equation 3

3. $b_m = \sqrt{\dfrac{\delta_p \rho_d (\partial w_m / \partial \varphi)}{p_{sat}}}$

For the SRE materials, a single value of $\partial w_m / \partial \varphi$ was calculated from the gradient of the straight line portion of the measured moisture storage function for each material (moisture capacity, ξ (see Hall and Allinson (2009) for more details).

Equations 2 and 3 result from an analytical solution of the mass transport between the test specimen and the air, and assume no boundary layer resistance. For this reason it is referred to as the 'ideal moisture buffer value' or MBV$_{ideal}$ and is the maximum possible value of the MBV. The results for the MBV$_{ideal}$ for each of the three SRE material types are presented in Table 2.

Where there is little air movement over the material's surface, the still boundary layer of air will increase surface moisture transfer resistance and the MBV will be lower than suggested by the analytical solution. To explore the relationship between the MBV and surface moisture transfer resistance, a numerical solution was developed.

Material	MBV$_{practical}$: g/m²%RH	MBV$_{ideal}$: g/m²%RH	MBV$_{simulation}$: g/m²%RH
613	0·68	1·54	1·35
433	0·61	1·11	1·00
703	1.29	1·61	1·43
Gypsum board	0·64[a]	2·46	1·88
Brick	0·48[a]	0·95	0·71
Spruce boards	1·16[a]	3·10	2·20

[a]Values from Nordtest (Rode, 2005)

Table 2. Summary of MBV

5. Numerical simulation of MBV

Combined heat and mass transfer equations, suitable for a numerical solution, are outlined in BS EN 15026:2007 (BSI, 2007). For this paper, a numerical solution of those equations was developed in the MathWorks Matlab high-level language. The program was named 'CHAMP' (for 'combined heat and mass in porous' materials). It utilised a time-marching, explicit finite-volume method to solve the discretised partial differential equations.

The total rate of heat transfer is considered to be the sum of the sensible and latent (due to vapour diffusion) heat transfer rates

4. $q = q_{sens} + q_{lat}$

The rate of sensible heat transfer is calculated using Fourier's law of heat conduction, where the thermal conductivity is a function of the moisture content and temperature increases with distance

5. $q_{sens} = -\lambda^* \dfrac{\partial T}{\partial x}$

The rate of latent heat transfer within the material and across boundaries is calculated from the rate of water vapour transfer and the specific latent enthalpy of evaporation (or condensation)

6. $q_{lat} = h_e g_v$

The value of enthalpy ($2 \cdot 45 \times 10^6$ J/kg) was assumed to be the same for both evaporation and condensation.

The total rate of mass transfer is calculated from the sum of the rates of water vapour and liquid water transfer

Construction Materials
Volume 165 Issue CM6

**Humidity buffering using
stabilised rammed earth
materials**
Allinson and Hall

7. $g = g_v + g_l$

The rate of water vapour transfer in the porous material is described by

8. $g_v = -\delta_p \dfrac{\partial p_v}{\partial x}$

The partial pressure of water vapour was calculated from the relative humidity (from the moisture storage function) using the relationship

9. $p_v = \phi 610{\cdot}5 e^{\frac{17{\cdot}269(T - 273{\cdot}15)}{T - 35{\cdot}85}}$

The experimentally measured water vapour diffusion resistance factor was used to describe the vapour permeability of the material in terms of the vapour permeability of still air at the same temperature and pressure

10. $\delta_p = \dfrac{\delta_a}{\mu}$

The vapour permeability of still air was calculated from the Schirmer formula

11. $\delta_a = \dfrac{2{\cdot}306 \times 10^{-5}}{R_{vap} T} \dfrac{P_0}{P_a} \left(\dfrac{T}{273{\cdot}15} \right)^{1{\cdot}81}$

The ratio of the standard atmospheric pressure (101 325 Pa) to the actual barometric pressure was assumed to be unity. Liquid moisture transfer was set to zero because the maximum relative humidity was 75% for the duration of the tests and hence mass transport would be governed by diffusion as opposed to capillary potential.

In order to simulate the time-varying one-dimensional hygro-thermal behaviours, the heat and mass transfer equations described above were combined using balancing equations derived from the conservation of energy and conservation of mass. Considering an elemental control volume of a porous building material, as shown in Figure 4, by conservation of heat energy, the rate of accumulated heat is a result of the net rate of heat transfer into that volume

12. $\left(\rho_d c_{pm} + w c_{pl} \right) \dfrac{\partial T}{\partial t} = -\dfrac{\partial q}{\partial x}$
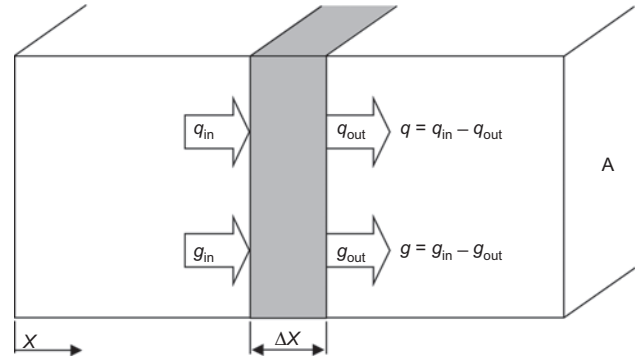

Figure 4. Simulated control volume in cross-section of wall

Similarly, by conservation of mass, the rate of accumulated moisture is a result of the net inflow rate of moisture

13. $\dfrac{\partial w}{\partial t} = -\dfrac{\partial g}{\partial x}$

The negative symbol on the right-hand side of each equation indicates that both heat and moisture will flow from areas of high potential to areas of lower potential. Each of these equations must be satisfied at every position within the material and at any time.

To solve the simultaneous partial differential equations described above, a numerical solution was used that divided the wall into discrete elements that could then be studied at discrete time steps. The schematic diagram in Figure 5 shows a notional building wall divided into a number of control volumes. The heat (energy) and moisture (mass) for each control volume were assumed to be stored at the central node. The resistance to the flow of heat between any two adjacent
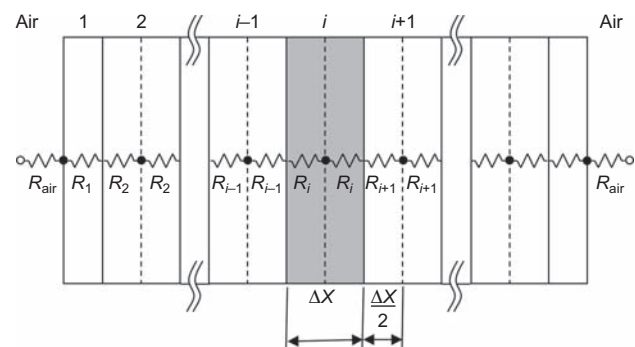

Figure 5. Simulated control volume resistances for finite-volume analysis

Construction Materials
Volume 165 Issue CM6

**Humidity buffering using
stabilised rammed earth
materials**
Allinson and Hall

nodes was described, using an electrical analogy, by two thermal resistors connected in series (see Figure 5). Each resistor represented half of the control volume such that

14. $\quad R = \dfrac{\Delta x / 2}{\lambda^*}$

By assuming small values of Δx such that $\Delta x \to \partial x$ and $\Delta T \to \partial T$ the resistances were substituted into the transport equation (Equation 5), to give the rate of sensible heat transfer for the ith control volume from its neighbouring volumes, subscripted $i - 1$ and $i + 1$

15. $\quad q_{\mathrm{sens},i} = \dfrac{T_{i-1} - T_i}{R_{i-1} + R_i} + \dfrac{T_{i+1} - T_i}{R_{i+1} + R_i}$

Similarly, the resistance to the flow of water vapour between each node and the edge of its control volume was calculated from the vapour permeability

16. $\quad R_{\mathrm{v}} = \dfrac{\Delta x / 2}{\delta_{\mathrm{p}}}$

Substituting these resistance values into their transport equation (Equation 8), gave the rates of water vapour transfer for the ith control volume

17. $\quad g_{\mathrm{v},i} = \dfrac{p_{\mathrm{v},i-1} - p_{\mathrm{v},i}}{R_{\mathrm{v},i-1} + R_{\mathrm{v},i}} + \dfrac{p_{\mathrm{v},i+1} - p_{\mathrm{v},i}}{R_{\mathrm{v},i+1} + R_{\mathrm{v},i}}$

The rate of latent heat transfer was then calculated from the water vapour flow (Equation 6)

18. $\quad q_{\mathrm{lat},i} = h_{\mathrm{e}} g_{\mathrm{v},i}$

By inserting these results into the heat and mass balances (Equations 12 and 13) and assuming small values of time step, Δt (s), such that $\Delta t \to \partial t$, these equations were written in a discrete form suitable for numerical analysis as follows

19. $\quad \left(\rho c_{\mathrm{pm}} + w_i^n c_{\mathrm{pl}} \right) \dfrac{T_i^{n+1} - T_i^n}{\Delta t} = \left[\dfrac{q_{\mathrm{sens},i} + q_{\mathrm{lat},i}}{\Delta x} \right]^n$

20. $\quad \dfrac{w_i^{n+1} - w_i^n}{\Delta t} = \left[\dfrac{g_{\mathrm{v},i}}{\Delta x} \right]^n$

In this way, the temperature and moisture content of the ith control volume were calculated at the next time increment, $t + \Delta t$ (parameters superscripted, $n + 1$) from the current temperature and moisture content and the induced heat and mass transfer (parameters superscripted, n). The computational algorithm used for the analysis is shown in Figure 6. The computer code was tested and successfully validated to the benchmark example in BS EN 15026:2007 (BSI, 2007), and the results were well within the specified accuracy limits ($\pm 2{\cdot}5\%$).

For the simulation of the MBV test, initial conditions were assumed to be 23°C and 53% RH. At time $t = 0$ the outside climate was adjusted to 75% RH and then 33% RH after 8 h. This was repeated on a 24 h cycle for 5 days. The 40 mm samples were divided into 101 control volumes. The first and last volume had half of the thickness of those within the wall and the node was located at the surface. Boundary conditions were introduced at both of the outside surfaces. For the first control volume (subscripted '1') the rate of water vapour diffusion depended upon the partial vapour pressure of the air (subscripted 'air') and its vapour resistance as well as those of the control volume and its neighbour (subscripted '2') such that
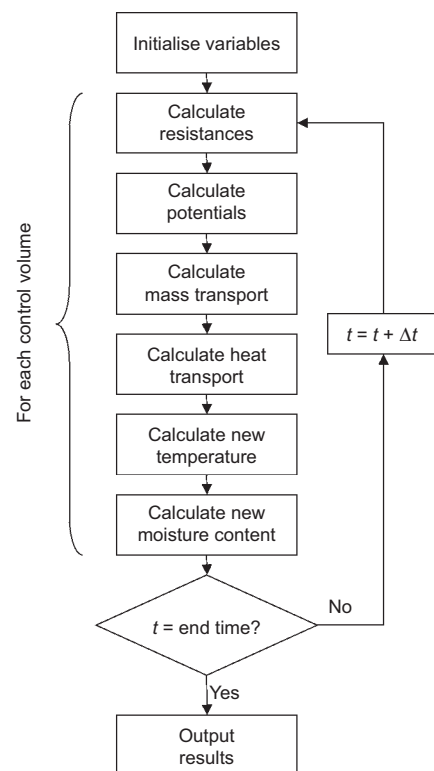

Figure 6. Flow chart of the computational algorithm

21. $\quad g_{v,1} = \dfrac{p_{v,air} - p_{v,1}}{R_{v,air}} + \dfrac{p_{v,2} - p_{v,1}}{R_{v,2} + R_{v,1}}$

Similarly, the rate of sensible heat transfer for the first control volume was calculated from the air temperature and the surface resistance

22. $\quad q_{sens,1} = \dfrac{T_{air} - T_1}{R_{air}} + \dfrac{T_2 - T_1}{R_2 + R_1}$

The rate of latent heat transfer was calculated from the water vapour flow in the usual way

23. $\quad q_{lat,1} = h_e g_{v,1}$

It was assumed that there was no heat or mass transfer for the last control volume as the samples were sealed on all but one surface. The surface resistances for convective heat transfer and moisture transfer were assumed to be 0·125 m^2 K/W and 5 × 10^7 m^2 s Pa/kg respectively, representing indoor surfaces and in agreement with the figures given by Nordtest. MBV values (MBV$_{simulation}$) were calculated from the resulting mass–time profiles in the same way as for the experimental tests and are presented in Table 2.

6. Results and discussion

Published results of MBV$_{practical}$ for gypsum board, brick and spruce timber boards (Rode, 2005) are included in Table 2 as well as values of MBV$_{ideal}$ and MBV$_{simulation}$ that were calculated from available published material properties (see Table 1 for values and source). This enabled direct comparison with the three SRE material types studied here.

The results demonstrate that SRE can have a wide range of MBV values, between moderate and good (moderate: 0·5–1·0 g/m^2%RH; good: 1·0–2·0 g/m^2%RH (Rode, 2005)). In this way, the authors suggest it would be possible to design the behaviour of the SRE walls intelligently to match the moisture fluxes that occur in a particular room and/or for a particular indoor climate or user pattern, chiefly by controlling PSD, mineralogy selection and compaction energy. This hypothesis also reinforces previous findings by the authors (Allinson and Hall, 2010). The results also support the anecdotal evidence that SRE walls do provide good levels of building integrated passive air conditioning. As the three SRE materials tested are not exhaustively representative, it is expected that further control of the grading, mineralogy and manufacturing of the material will lead to a much wider range of MBV$_{practical}$ values. An additional advantage of SRE materials is that it is usual to leave their surface exposed to

the indoor air, unlike concrete, brick, plaster and timber which are all traditionally covered, painted or varnished; reducing vapour permeability and their effectiveness. The geometry of any exposed material (surface area and material thickness), as well as the temperature profile in the room, would also have to be considered in any analysis to optimise thermal and humidity buffering.

It can be seen from Table 2 that MBV$_{ideal}$>MBV$_{simulation}$>MBV$_{practical}$, in all cases. To explore the uncertain relationship between the values, the MBV was simulated for each of the materials at a number of different surface moisture transfer resistances, as shown in Figure 7. It can be seen from the figure that the simulated moisture buffer value (MBV$_{simulation}$) decreased with increasing surface resistance and that the maximum value (when surface resistance = 0) was the same as the analytical result (MBV$_{ideal}$). As surface resistance increased, the rate of decrease in the simulated MBV was higher for materials with a higher MBV, until the results for all materials tend towards a similar value, below 0·5 g/m^2%RH. A useful indicator of this sensitivity is the moisture Biot number, being the ratio of the moisture resistance of the material to that of the surface film, as described in Nordtest (Rode, 2005).

The MBV was measured at a surface resistance of (5 × 10^7 m^2 s Pa/kg), as indicated by the grey line on the graph in Figure 7. The uncertainty in the surface moisture transfer resistance in experimental testing will have a greater impact on the uncertainty of the measured MBV values for materials with a higher MBV. However, the variation between the measured and simulated values cannot be simply explained by the uncertainty in the surface resistance. Additional measurement uncertainty will affect both the measured result and the values of the functional properties that are used in the analytical and numerical solutions. This is further compounded by the heterogeneity of construction materials and any variations between samples. These results suggest that careful experimental control and averaging of the results from tests on large numbers of samples would be needed to improve confidence.

As hardened cement paste typically contains meso-pores (2–50 nm) and some macro-pores (>50 nm), these additional pores will not have a significant effect on Fickian vapour diffusion but the increased volume of hydrated cement paste could produce a slight pore blocking effect. Since the samples were a minimum of 28 days old at the time of testing, additional hydration caused by vapour absorption is less likely to affect transport behaviour than in early age samples and any changes in pore structure would most likely be restricted near to the surface (<10 mm depth). Further study would be required in order to characterise the extent of such microstructural alterations.

Construction Materials
Volume 165 Issue CM6

Humidity buffering using
stabilised rammed earth
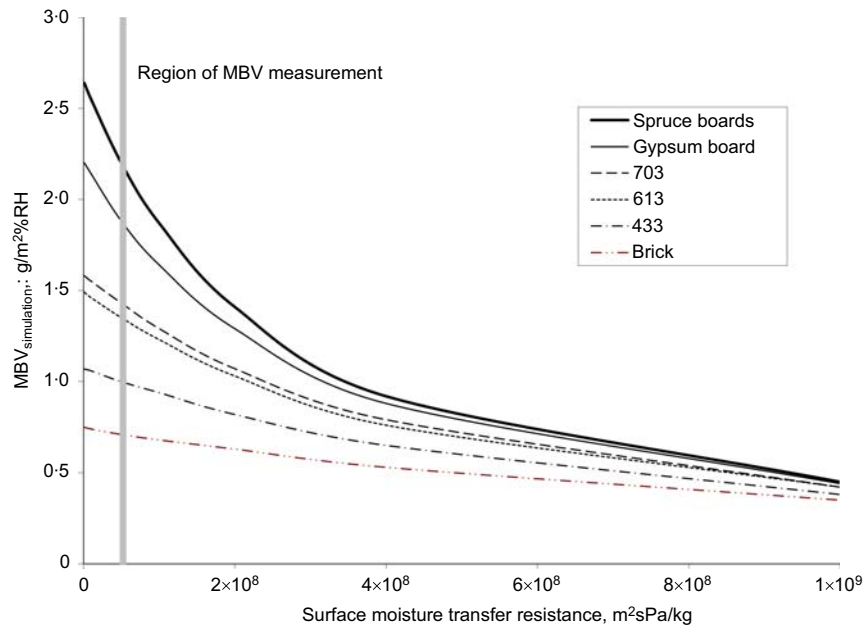materials
Allinson and Hall

Figure 7. Simulated variation in MBV with surface moisture
transfer resistance

7. Conclusion and future work

The results of measuring the MBV of three representative SRE
material types indicate that SRE can be a good moisture
buffering material. Variations in the result between the three
mix designs indicate that there is scope for designing the SRE
material to maximise its passive air-conditioning potential in a
given space. A validated numerical solution (i.e. CHAMP) of
the combined heat and mass transfer equations, using a time-
marching, explicit, finite-volume method to solve the discre-
tised partial differential equations has been developed.
Analysis using this model indicated that materials with higher
MBV show a greater decrease in MBV with increasing surface
moisture transfer resistance.

Further work is needed to improve the reliability of the MBV
measurements by carefully controlling the experimental con-
ditions. These experimental results can then be used as further
validation of hygrothermal simulations. The relationship
between the grading, mineralogy and manufacturing of SRE
materials, and how these relate to material functional proper-
ties, determines how the MBV might be optimised to suit a
particular application and also the origins of their hygro-
thermal functional properties. Ultimately, the use of SRE walls
to control relative humidity and condensation in buildings
could improve occupants' thermal comfort, prevent damage to
contents and fabric, improve indoor air quality and save
energy.

Acknowledgements

REFERENCES

Allinson D and Hall M (2010) Hygrothermal analysis of a
   stabilised rammed earth test building in the UK. *Energy
   and Buildings* **42(6)**: 845–852.

BSI (1990) BS EN 1377-4: Methods of test for soils for civil
   engineering purposes. Compaction-related tests. BSI,
   London, UK.

BSI (2007) BS EN 15026: Hygrothermal performance of
   building components and building elements – assessment of
   moisture transfer by numerical simulation. BSI, London,
   UK.

CIBSE (Chartered Institute of Building Service Engineers) (2006)
   CIBSE Guide A: Design Data. Chartered Institute of
   Building Service Engineers, London, UK.

Fang L, Clausen G and Fanger PO (1998a) Impact of
   Temperature and humidity on perception of indoor air
   quality during immediate and longer whole-body
   exposures. *Indoor Air* **8(4)**: 276–284.

Fang L, Clausen G and Fanger PO (1998b) Impact of temperature
   and humidity on the perception of indoor air quality.
   Indoor Air **8(2)**: 80–90.

Hall M and Allinson D (2009) Analysis of the hygrothermal

Construction Materials
Volume 165 Issue CM6

**Humidity buffering using
stabilised rammed earth
materials**
Allinson and Hall

functional properties of stabilised rammed earth materials. *Building and Environment* **44(9)**: 1935–1942.

Hall M and Djerbib Y (2004) Rammed earth sample production: context, recommendations and consistency. *Construction and Building Materials* **18(4)**: 281–286.

Howieson SG, Lawson A, Mcsharry C *et al*. (2003) Domestic ventilation rates, indoor humidity and dust mite allergens: are our homes causing an asthma pandemic. *Building Services Engineering Research and Technology* **24(3)**: 137–147.

Kurnitski J, Kalamees T, Palonen J, Eskola L and Seppanen O (2007) Potential effects of permeable and hygroscopic lightweight structures on thermal comfort and perceived IAQ in a cold climate. *Indoor Air* **17(1)**: 37–49.

Mendonca P (2007) Non-structural adobe walls in housing building – environmental performance. *Proceedings of the International Symposium on Earthen Structures*. Interline Publishing, Bangalore, India.

Minke G (2000) *Earth Construction Handbook : The Building Material Earth in Modern Architecture*. WIT Press, Southampton, UK.

Mortenson N (2000) *The Naturally Air Conditioned House,* latest update. See http://www.dab.uts.edu.au/ebrf/research/air_conditioned.html (accessed 08/04/2010).

Oreszczyn T, Ridley I, Hong SH, Wilkinson P and Warm Front Study Group (2006) Mould and winter indoor relative humidity in low income households in England. *Indoor and Built Environment* **15(2)**: 125–135.

Osanyintola OF and Simonson CJ (2006) Moisture buffering capacity of hygroscopic building materials: experimental facilities and energy impact. *Energy and Buildings* **38(10)**: 1270–1282.

Padfield T (1998) *The Role of Porous Building Materials in Moderating Changes of Relative Humidity*. Technical University of Denmark, Kongens Lyngby, Denmark.

Rode C (2005) *Moisture Buffering of Building Materials*. Technical University of Denmark, Kongens Lyngby, Denmark, BYG DTU R-126.

Simonson CJ, Salonvaara M and Ojanen T (2002) The effect of structures on indoor humidity – possibility to improve comfort and perceived air quality. *Indoor Air* **12(4)**: 243–251.

Taylor P and Luther MB (2004) Evaluating rammed earth walls: a case study. *Solar Energy* **76(1–3)**: 79–84.